Bull. Chem. Soc. Ethiop. **2023**, 37(3), 633-651.
DOI: https://dx.doi.org/10.4314/bcse.v37i3.8

ISSN 1011-3924
Printed in Ethiopia
Online ISSN 1726-801X

ZINC(II) COMPLEX OF (Z)-4-((4-NITROPHENYL)AMINO)PENT-3-EN-2-ONE, A POTENTIAL ANTIMICROBIAL AGENT: SYNTHESIS, CHARACTERIZATION, ANTIMICROBIAL SCREENING, DFT CALCULATION AND DOCKING STUDY

I. Waziri[1*], O. O. Wahab[2*], G. A. Mala[1], S. O. Oselusi[3], S. A. Egieyeh[3] and H. Nasir[4]

[1]Department of Pure and Applied Chemistry, University of Maiduguri, P.M.B. 1069, Maiduguri, Borno State, Nigeria
[2]Department of Chemistry, Faculty of Natural and Applied Sciences, Nigerian Army University Biu, P.M.B. 1500, Biu, Nigeria
[3]School of Pharmacy, University of the Western Cape, Bellville, Cape Town, 7535, South Africa
[4]Department of Science Laboratory Technology (SLT), Ramat Polytechnics Maiduguri, Nigeria

(Received August 15, 2022; Revised October 4, 2022; Accepted December 20, 2022)

ABSTRACT. Herein, the synthesis and characterizations of (*Z*)-4-((4-nitrophenyl)amino)pent-3-en-2-one (HL) ligand and its Zn(II) complex are reported. The compounds were characterized using elemental and thermogravimetric (TGA) analysis, electrochemical studies, FTIR, UV-Vis, ^{1}H and ^{13}C{H}NMR, HRMS, and PXRD techniques. Antimicrobial activity was screened on some Gram-positive and Gram-negative bacteria. DFT predictions were achieved using B3LYP, ωB97XD and M06-2X functional with 6-31+G(d,p) and LANL2DZ basis sets for nonmetallic and metallic atoms, respectively. The therapeutic potentials of the compounds were evaluated based on protein binding affinity, ADME/T and drug-likeness properties. The experimental results revealed the formation of a complex in which two ligands coordinated to the zinc ion in a tetrahedral arrangement through their carbonyl and amino groups. The antimicrobial study showed that the complex possesses higher antimicrobial activity than free ligand and the control (Streptomycin). B3LYP emerged as the best performing functional having yielded the best IR spectra and geometrical parameters relative to the experimental data. The density functional theory (DFT) predictions revealed that the complex is more active than the ligand, and its formation is thermodynamically feasible and exothermic. The docking results revealed that the binding affinities of the compounds are in agreement with the *in-vitro* data, and they possess drug-like properties.

KEY WORDS: Schiff base, Zinc complex, Antimicrobial, DFT, Docking study

INTRODUCTION

Schiff bases are important classes of organic compounds with numerous interesting applications [1]. They are generally synthesized via condensation reactions between amino compounds and aldehydes or ketones which produce an azomethine group. Being one of the most widely used ligands in coordination chemistry, Schiff bases have continued to receive attention due to their facile synthesis, stability, and ease of coordination [2-4]. They coordinate to different metals through azomethine nitrogen and their coordination chemistry plays a significant role in organic synthesis, analytical chemistry, electrochemistry, pharmaceuticals, etc [5-7]. Different Schiff bases present unique properties depending on the component aldehydes or ketone, but their applications remain similar due to their possession of a common (azomethine) functional group. Acetylacetonate-based Schiff base ligands and their metal complexes have widespread applications in science and engineering [8].

Schiff bases derived from β-diketones can exist either as β-ketoamine or β-ketoimine tautomeric form. However, the β-ketoamine analogue (which bears a =C–NH–) is more stable than the β-ketoimine counterpart (which bears a –C=N–). Therefore, Schiff bases of this type are

*Corresponding author. E-mail: waziriibrahim@unimaid.edu.ng and olaide.wahab@naub.edu.ng

usually presented as having (=C–NH–) instead of (–C=N–). These compounds are fascinating class of *NO* donor bidentate ligands that can be easily adjusted to fine-tune the steric and electronic effects around metal centres, due to two opposing features exhibited by the donor atoms (soft and hard donors) [9, 10].

The acetylacetonate Schiff base considered for this study is (*Z*)-4-((4-nitrophenyl)amino)pent-3-en-2-one (HL). This compound which uses acetylacetone and 4-nitroaniline as precursors had previously been reported with its crystal structure [11]. However, to the best of our knowledge after an in-depth exploration of the literature, there is no account of its complexation with Zn(II) ion and/or its biological applications either as a free ligand or in complex with the metal ion. Interestingly, a similar ligand (derived from acetylacetone and 2-amino-5-glunidinopentanic acid) and its Cu(II), Co(II), Ni(II) and Zn(II) complexes have been found to possess enhanced biological properties [12]. This suggests that Schiff bases of acetylacetone and their metal complexes might offer better antimicrobial property.

Given the prevalence of microbial resistance to existing antibiotics [4-7], development of stronger antibiotic compounds for combating the menace of dangerous microorganisms becomes imperative. Therefore, we reported in this work the syntheses, characterizations and antimicrobial properties of (*Z*)-4-((4-nitrophenyl)amino) pent-3-en-2-one (HL) and its Zn(II) complex. The aim is to develop a more potent antimicrobial agent which can be used to overcome the problem of antimicrobial resistance.

EXPERIMENTAL

Materials

All chemicals and solvents used were of analytical grade (AR) and used without further purifications.

*Synthesis of (Z)-4-((4-nitrophenyl)amino)pent-3-en-2-one (**HL**)*

The Schiff base ligand was synthesized using a modified form of an existing procedure [13]. To a hot methanolic (20 mL) solution of 4-nitroaniline (1.3812 g, 10 mmol, 1 eq), a hot methanolic (10 mL) solution of acetylacetone (1.0031 g, 10 mmol, 1 eq) was added dropwisely with constant stirring, followed by addition of five drops of formic acid to the mixture. The mixture was stirred at room temperature for 6 h, after which a yellow precipitate was formed. The solid product was washed with cold ether several times and crystallized in hot methanol to give a yellow needle-like crystal (Scheme 1). Yield: (1.36 g, 62.7%), mp: 140–142 °C. ^{1}H NMR (400 MHz, DMSO-d_6), δ(ppm): 2.06 (s, 3H, CH_3), 2.22 (s, 3H, CH_3), 5.44 (s, 1H, CH), 7.39 (d, 2H, J_{HH} = 9.2 Hz, Ar-H), 8.18 (d, 2H, J_{HH} = 9.2 Hz, Ar-H), 12.66 (s, 1H, NH); ^{13}C{H}NMR (101 MHz, DMSO-d_6), δ (ppm): 20.1 (CH_3), 29.4 (CH_3), 100.9 (CH), 121.8, 125.1, 142.6, 145.1, (ArC), 157.3 (C-N), 196.9 (C=O); IR_{ATR}: 2970, 1620, 1566, 1481, 1280, 1257, 1188, 1103, 1018, 918, 833, 786, 748, 686, 609, 516, 493 cm^{-1}; CHN anal. calculated for $C_{11}H_{12}N_2O_3$: C, 59.99; H, 5.49; N, 12.72; found C, 59.92; H, 5.49; N, 12.87, HRMS-ESI *m/z* $[M+H]^+$ 224.1103 (calculated for $C_{11}H_{12}N_2O_3$ 222. 0960).

*Synthesis of bis (Z)-4-((4-nitrophenyl)amino)pent-3-en-2-one zinc(II) complex [**ZnL$_2$**]*

To a 15 mL of a methanolic solution of the ligand (0.4482 g, 2 mmol, 2 eq), a 15 mL of methanolic solution of zinc nitrate hexahydrate (0.2975 g, 1 mmol, 1 eq) was added dropwisely with continuous stirring after which three drops of triethylamine was added (to adjust the pH, and improve the solubilization of the ligand in methanol *via* deprotonation of the amine proton). The mixture was refluxed at 60 °C for 12 h and the progress of the reaction was monitored by thin-

layer chromatography (TLC). At the end of the reaction, the yellow solution obtained was cooled overnight in the refrigerator. The pale yellow solid product (complex) formed was filtered, washed with cold methanol, and diethyl ether, and dried in a vacuum desiccator over anhydrous calcium chloride (Scheme 1). Yield: (0.16 g, 68.2%); mp: 268 °C. ^{1}H NMR (400 MHz, DMSO-d_6), δ(ppm): 1.76 (s, 3H, CH_3), 1.94 (s, 3H, CH_3), 5.09 (s, 1H, CH), 6.89 (d, 2H, J_{HH} = 8.8 Hz, Ar-H), 8.14 (d, 2H, J_{HH} = 9.2 Hz, Ar-H); ^{13}C{H}NMR (101 MHz, DMSO-d_6), δ(ppm): 22.8 (CH_3), 27.7 (CH_3), 98.1 (CH), 124.6, 124.8, 143.9, 154.1, (ArC), 171.8 (C-N), 187.1 (C=O); IR_{ATR}: 1558, 1512, 1388, 1334, 1257, 1203, 1103, 1018, 933, 879, 802, 763, 709, 686, 632, 563, 509, 447, 416 cm^{-1}; CHN anal. calculated for $C_{22}H_{22}N_4O_6Zn$: C, 52.45; H, 4.40; N, 11.12; found C, 52.33; H, 4.37; N, 11.06. HRMS-ESI *m/z* $[M-H]^-$ 501.0876 (calculated for $C_{22}H_{22}N_4O_6Zn$ 501.0831).

Measurements

NMR spectra were recorded on a Bruker 400 MHz spectrometer. Chemical shifts were reported as parts per million (ppm) relative to tetramethylsilane (TMS) in DMSO-d_6. All NMR analyses were conducted at room temperature. Infrared spectra were recorded on a Tensor 27 Bruker and Perkin-Elmer FT-IR spectrometer BX. Elemental analyses were performed on a VarioElementar III microbe CHN analyzer. Electronic absorption spectra in 200-800 nm range were obtained in DMF (10^{-3} M solution) on a UV-visible spectrometer at room temperature. Powder X-ray diffraction (PXRD) data were collected at 40 keV, 15 mA on a Rigaku Mini-Flex 600 Bench-top diffraction using Cu-Kα radiation (ƛ = 1.5418Å) over 2Ɵ range of 0-80 °C at room temperature. Thermogravimetric analysis (TGA) was carried out on a TGA-Q600 thermoanalyzer with a heating rate of 10 °C min^{-1} under nitrogen flow.

Electrochemical studies

The electrochemical measurements were carried out using a Biologic SP-200 Computer-controlled electrochemical measurement device with a potentiostat. A three-electrode system comprising of a glassy carbon working electrode, a platinum wire counter electrode and a saturated Ag/AgCl in KCl reference electrode was used for this study with a 0.01 M phosphate buffer solution (PBS) of pH 7.4 as a supporting electrolyte.

In-vitro antimicrobial studies

The synthesized ligand and its complex were evaluated for antimicrobial activity against *Staphylococcus aureus* ATCC-25923 (Sa), *Streptococcus pyogene* ATCC-19615 (Sp) *Escherichia coli* ATCC-25922 (Ea), and *Klebsiella pneumoniae* ATCC-13883 (Kp), using a modified filter paper disc agar diffusion method [14]. The activities of the compounds towards the selected bacteria were evaluated relative to a standard (streptomycin). The test was conducted in triplicate and the results were presented as mean ± SEM.

Determination of minimum inhibitory concentration (MIC)

The MIC of the compounds was assessed using the broth micro dilution method [15]. The MICs were assessed visually after the corresponding incubation period and were taken as the lowest sample concentration at which there was no microbial growth. Streptomycin (Sigma-Aldrich, Steinem, Germany) was used as positive controls, while broth with 20 µL of DMSO was used as a negative control to determine their influence on the biological systems. The assay was repeated thrice.

Computational studies

DFT calculations

The DFT study is primarily focused on predicting the relative reactivity, polarity, and thermodynamic stability of the synthesized complex. For this purpose, the performances of three high-level functionals namely: B3LYP, ωB97XD, and M06-2X were assessed based on their capacity to reproduce the experimental IR spectra of both the ligand and the complex. B3LYP is a hybrid functional derived from Becke exchange [16] and Lee-Yang-Par correlation functional [17]. ωB97XD is a dispersion corrected hybrid functional developed by Head-Gordon and co-workers [18] while M06-2X is a hybrid meta-GGA functional of the Truhlar group [19]. These functionals were used in conjunction with 6-31+G(d,p) and LANL2DZ basis sets for describing nonmetallic and metallic atoms, respectively [20]. Solvent phase calculations were performed implicitly in methanol using the integral equation formalism polarizable continuum model (IEFPCM) [21]. All DFT calculations were performed using Guassian 09 program with GaussView 05 as the visualizer [22].

The geometries of the ligand and the complex were prepared in GaussView 05 and subjected to full optimization with frequency calculation in the absence of symmetry contraint. No imaginary frequency was present in their vibrational frequency data. The predicted IR spectra of the ligand and the complex were obtained, and the absolute deviations (IR_{Dev}) from the experimental data were calculated using Equation 1. Relative reactivity was determined based on HOMO-LUMO energy gap (ΔE) and electro negativity (χ) calculated using Equations 2 and 3 [23, 24]. Polarity hence solubility of the compounds was predicted based on their dipole moment magnitudes. Thermodynamic stability was predicted from the change in free energy of complex formation (ΔG) obtained from the changes in enthalpy (ΔH) and entropy (ΔS) at 298.15 K using Equation 4.

$$\mathrm{IR_{Dev}} = \left|IR_{Predicted} - IR_{Expt}\right| \quad (1)$$

$$\Delta \mathrm{E} = \mathrm{E}_{LUMO} - \mathrm{E}_{HOMO} \quad (2)$$

$$\chi = \frac{1}{2}(\mathrm{E}_{LUMO} + \mathrm{E}_{HOMO}) \quad (3)$$

$$\Delta \mathrm{G} = \Delta \mathrm{H} - \mathrm{T}\Delta \mathrm{S} \quad (4)$$

Molecular docking studies of HL and ZnL_2 against selected bacteria proteins

The docking studies were performed on the PyRx software program (version 0.8). Using the "Open Babel widget" feature, the structures of the synthesized compounds HL and ZnL_2, and the reference drug (streptomycin) were imported. The compounds were energy minimized with Universal Force Field (UFF) using the conjugate gradient optimization algorithm with the total number of steps set at 200. The X-ray crystal structure of key protein targets in *Staphylococcus aureus* (1ESF)*, Streptococcus pyogenes* (6OG4)*, Klebsiella pneumonia* (6CN7), and *Escherichia coli* (1R4P) was obtained from the Protein Data Bank (PDB) web server (http://www.RCSB.org) and prepared for docking using the dock prep toolbar on UCSF Chimera software [25]. Thereafter, the minimized structures of both the ligands and proteins were converted to ready-to-dock PDBQT format on the PyRx program [26, 27]. Docking calculation was run at exhaustiveness of 8 and keeping other parameters as default. The conformation with the lowest (i.e. most negative) binding energy (kcal/mol**)** was selected and analyzed using PyMol (version 2.5) software [28].

Physicochemical, pharmacokinetics, and drug-likeness analysis

The study was performed using the SwissADME web tool (http://www.swissadme.ch/) developed by the Swiss Institute of Bioinformatics [29, 30] and OSIRIS DataWarrior software [29, 31]. The SMILES structures of the compounds were prepared using ChemDraw [32] and then pasted into the SwissADME web server. Key physicochemical properties such as molecular weight, lipophilicity, hydrogen bond counts, polar surface area, etc. were calculated while the drug-likeness properties of the compounds were estimated based on Lipinski's rule of five (RO_5) and Veber's rule as described in previous studies [33, 34]. Finally, the pharmacokinetic parameters namely absorption, distribution, metabolism, excretion (ADME), and toxicity (T) were determined to predict the fate of the compounds in human subjects.

RESULTS AND DISCUSSION

The Schiff base (HL) was synthesized by the condensation of 4-nitroaniline and acetylacetone in methanolic solution at room temperature in a 1:1 mole ratio. The corresponding Zn(II) complex was obtained after the reaction of the ligand with zinc nitrate hexahydrate in a 1:2 mole ratio of metal to the ligand (Scheme 1). Both the ligand and the complex gave moderate yield and are stable at room temperature. The ligand and the complex were obtained as yellow and light-yellow compounds, respectively. The ligand is soluble in methanol, ethanol, acetonitrile, dichloromethane, dimethylformamide, and dimethyl sulfoxide, while the complex is only soluble in acetonitrile, dimethylformamide, and dimethyl sulfoxide. This suggests that the complex is slightly less polar than the ligand. Spectroscopic and analytical data obtained are in good agreement with the proposed structures and molecular formula. The positions of the molecular ion peaks in the mass spectra of the ligand and the complex are consistent with their molecular weights and formula. The molar conductivity (K) value of 15.3 $\Omega^{-1}cm^2mol^{-1}$ was obtained for the complex in DMF, suggests that the complex is less electrolytic in this solvent [35].

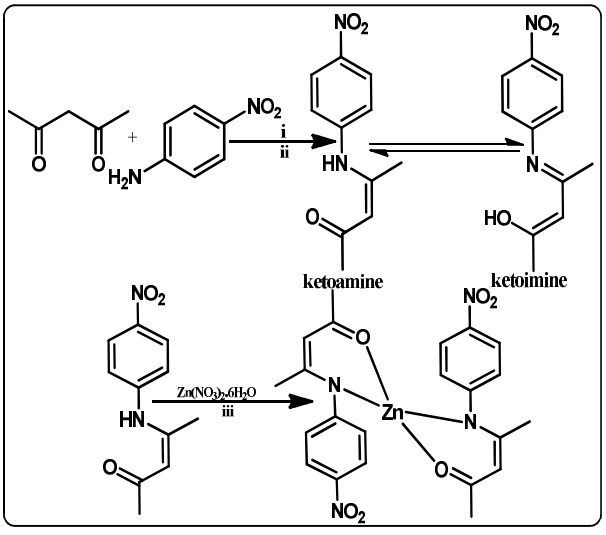

Scheme 1. Synthesis of the ligand and its Zn(II) complex; i = CH_3OH/HCOOH; ii = RT, 6 h; iii = CH_3OH/Et_3N; 60 °C, 12 h.

^{1}H and $^{13}C\{H\}$NMR

The ^{1}H NMR and ^{13}C{H}NMR spectra for HL and its Zn(II) complex obtained in DMSO-d_6. The ^{1}H NMR spectrum of the ligand shows a single broad peak downfield 12.66 ppm, corresponding to the proton of the amine group (N-H). The protons of the methyl substituents in the ligand appeared upfield between 2.06 and 2.22 ppm as singlet peaks due to differences in chemical environments as a result of the involvement of the carbonyl group in the formation of β-ketoamine. The vinylic proton appeared as a singlet at 5.44 ppm.

The ^{13}C{H}NMR spectrum of the ligand presents a signal for the sp^2 carbon of the ketone functional group at 196.98 ppm, the carbon bonded to the amine function at 157.31 ppm, the vinylic carbon at 100.99 ppm and the aromatic carbons of the phenyl ring at 121.84-145.18 ppm. The methyl carbon appeared at 29.45 and 20.18 ppm, respectively, due to the difference in their chemical environments as a result of the formation of β-amine function. Upon complexation with Zn(II) ion, significant changes in the ^{1}H NMR spectrum were observed. The methyl protons which initially appeared as singlet at 2.06 and 2.22 ppm shifted to 1.76 and 1.94 ppm, respectively, in the complex, and integrating to three protons, each in a different chemical environment. The appearance of these protons upfield as compared to their position in the free ligand suggests that the coordination to the metal ion occurred through the oxygen and nitrogen atoms of the carbonyl and amine, respectively. The vinylic proton also shifted upfield at 5.09 ppm due to complexation. The complete disappearance of the amine proton signal from the spectrum of the complex indicates that the ligand is deprotonated before coordination to the metal ion. The aromatic protons appeared upfield as duplets with each integrating into two protons. These changes in positions of the proton signals confirm the formation of the complex.

Similarly, the ^{13}C{H}NMR spectrum of the complex shows substantial changes in the positions of the carbon signals upon complex formation. The carbon atoms of methyl groups appeared at 22.8 and 27.7 ppm, the vinyl carbon at 98.0 ppm and the aromatic carbon at 124.6-154.1 ppm. In addition, the carbon bonded to the amine function shifted downfield to appear at 171.8 ppm against the 157.3 ppm observed in the free ligand while the sp^2 carbon of the ketone functional group shifted upfield appearing at 187.1 ppm as opposed to the 196.9 ppm obtained for the ligand. The changes in the positions of these two carbons confirm the involvement of the amine nitrogen and the carbonyl oxygen in coordination.

Infrared spectral studies

To investigate the functional groups within the ligand, and establish their involvement in coordination to the Zn(II) ion, IR spectra of the free ligand and its complexes were obtained in the region of 4000-400 cm^{-1} as depicted in Figure 1. The presence of a free $–NH_2$ group in a compound is usually signalled at 3400 cm^{-1}. Therefore, the absence of this band from the spectra of the ligand and the presence of broad band around 3100 cm^{-1} which is assignable to N–H stretching vibration confirm the successful formation of β-ketoamine, not β-ketoimine [36]. Other supporting evidence include the appearance of ν(C=O) band at 1620 cm^{-1}, the ν(C-N) band at 1526 cm^{-1} and the absence of a ν(C=N) band around 1690-1640 cm^{-1}.

The IR spectrum of the complex differs significantly from that of the free ligand (Figure 1). The ν (N-H) band initially observed at 3100 cm^{-1} for the free ligand is completely absent in the complex due to deprotonation of the amine group and subsequent coordination to the metal ion through the nitrogen atom. The shift of ν(C-N) and ν(C=O) bands from 1526 cm^{-1} to 1334 cm^{-1} and 1620 cm^{-1} to 1504 cm^{-1}, respectively, confirms the involvement of the carbonyl oxygen and the amine nitrogen atom in the coordination. In addition, appearance of two new bands at 428 cm^{-1} and 563 cm^{-1}, assignable to ν(M-N) and ν(M-O) [37-39], respectively, further confirms the involvement of the amine and the carbonyl groups in the formation of the complex. The result of the theoretical IR data correlates well with this experimental data.

Electronic absorption spectra

The electronic absorption spectra of the free ligand and the complex are shown as Figure 1. It can be seen that the ligand displayed two bands at 280 and 320 nm, due to $\pi \rightarrow \pi^*$ and $n \rightarrow \pi^*$ transitions arising from the aromatic and amine moieties. The Zn(II) complex showed two distinct bands at 293 and 380 nm which are assignable to $\pi \rightarrow \pi^*$ and charge transfer from ligand to metal ion (LMCT), respectively, in a tetrahedral geometry [40-42]. Zinc complexes are generally diamagnetic due to the filled d-orbital. Hence, a d–d transition possibility is ruled out. The molar extinction coefficients (ε) of the ligand and complex were found to be 4000 and 2000 $cm^{-1}mol^{-1}$, respectively which correlate well with the observed colours.

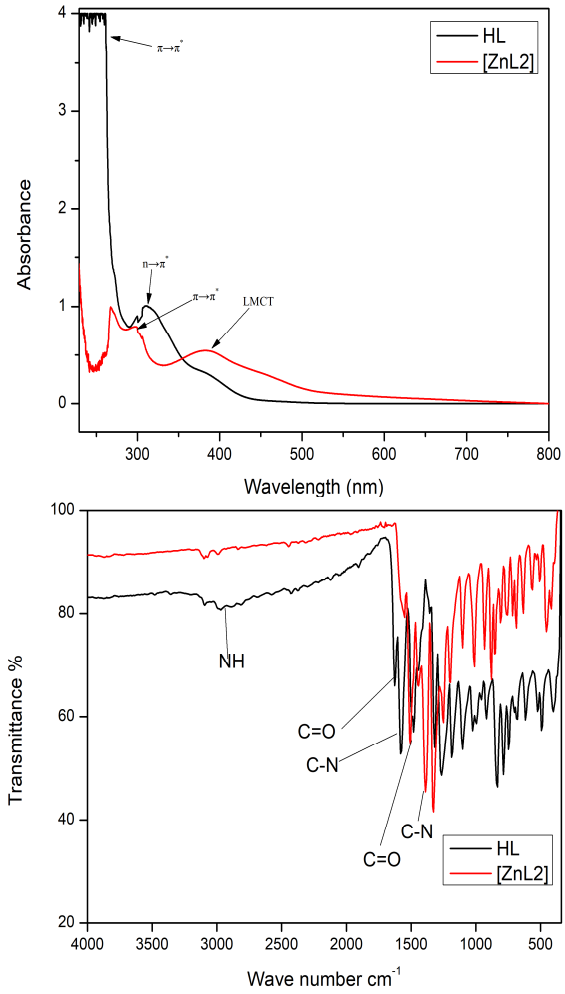

Figure 1. Plot of the electronic absorption (left) and FTIR (right) spectra of the ligand and its complex.

Thermal analysis

Thermal analysis is a useful technique for the determination of the crystal water content of complexes as well as their thermal stability/decomposition pattern under controlled heating. The thermal behaviours of the ligand and its complex as a function of temperature were studied by thermogravimetric analysis (TGA) over a temperature range of 20–800 °C. The obtained thermograms depicted in Figure 2 shows the weight losses recorded over the studied temperature range. The decomposition pattern of the ligand shows a two-step process: loss of -$C_{11}H_{12}NO^{*}$ radical at 0–160 °C and loss of the inorganic residue containing NO_2 at 160–400 °C. On the other hand, the thermogravimetric profile of the complex shows a three-step process, beginning with loss of the moisture content in the complex at 0–100 ºC, followed by loss of two ligand molecules and finally, the loss of inorganic residue containing NO_2 coupled with the formation of ZnO. It can thus be inferred from these results that both the ligand and the complex possess good thermal stability with the latter being more stable.

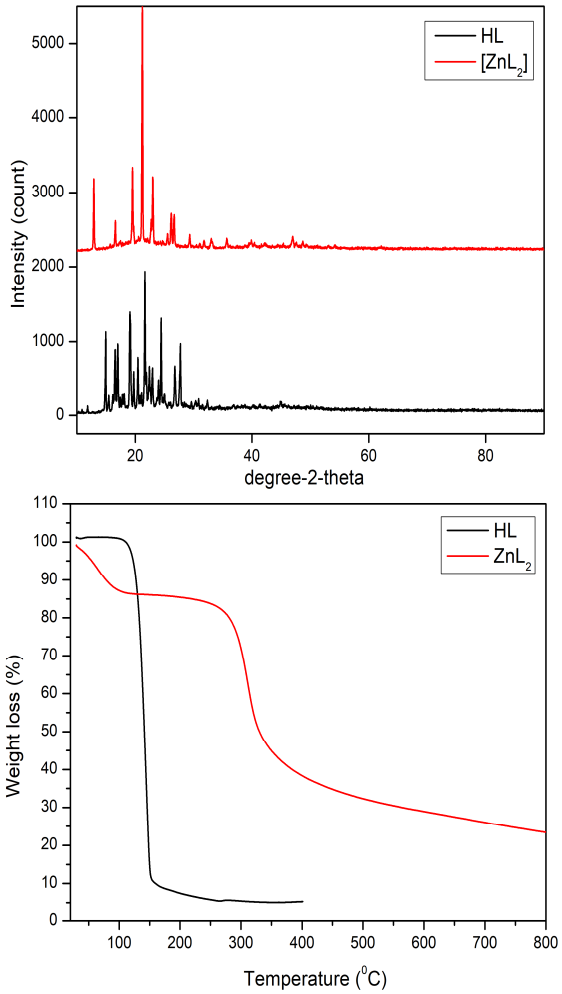

Figure 2. The PXRD spectra (left) and TGA thermogram (right) of the ligand and its complex.

X-Ray powder diffraction studies

An X-ray powder diffraction study was carried out on the synthesized compounds. The compounds were scanned in the range 2Θ = 0-80 °C at a wavelength of 15406 Å and the resulting diffraction patterns are shown in Figure 2. The sharp peaks and line broadening observed for the ligand and its complex indicate that they are crystalline. A single crystal X-ray crystallography would provide a more precise information about the crystal structures of these compounds. Unfortunately, several attempts made to obtain a single crystal of each compound for data collection were futile. However, the peaks of the complex are more clearly resolved compared to the ligand which might be due to the relatively smaller crystalline size of the complex. Generally in smaller crystalline complexes, there are no enough planes to produce destructive interference hence, broad space exists between their spectral peaks [43].

Mass spectra

To further confirm the formation of the Schiff base (HL) and its Zn(II) complex, the compounds were studied using ESI-MS. The proposed molecular formula of the ligand and its complex were ascertained by comparing them with *m/z* values. In the spectrum of the ligand, the molecular ion peak: *m/z* $[M+H]^+$ was found to be 224.1103 while the spectrum of the complex showed molecular ion peak: *m/z* $[M-H]^-$ at 501.0876. These data are in good agreement with the proposed molecular formula of the compounds. In addition, the mass spectrum of the ligand shows a single peak, suggesting that the compound is stable, while the spectral peaks of the complex confirm its decomposition patterns as revealed by thermal analysis.

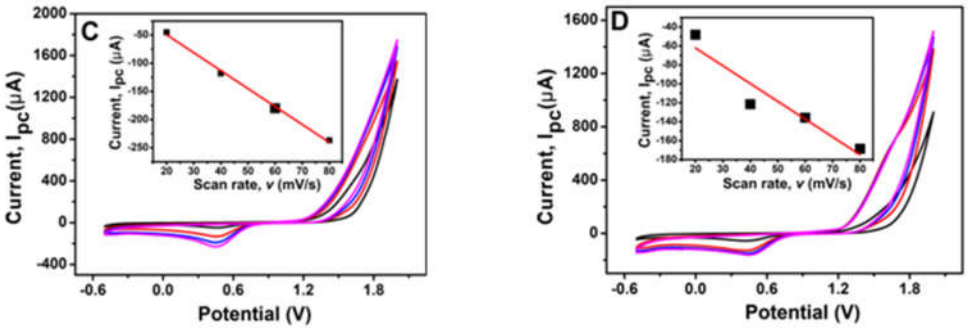

Figure 3. Cyclic voltammograms of HL (C) and ZnL_2 (D). Inset: calibration curve of I_{pc} versus *v* at scan rates 20, 40, 60, and 80 mVS^{-1} in 0.01 M PBS, pH 7.4.

Electrochemical studies

Redox behavior of metal ions is an important determinant of their biological properties. Redox active metals show better biological activity compared to redox inactive metals. To investigate the electrochemical properties of the synthesized compounds, ascertain their redox behavior and compare with the antimicrobial study, both the ligand and the complex were studied by cyclic voltammetry (CV) in a 0.01 M PBS electrolyte at scan rates 20, 40, 60, 80 mVS^{-1}. The results obtained are displayed as Figure 3C-D for the ligand and the complex, respectively. The single reductive wave observed for the ligand between -0.5 V and 2.0 V potentials (Figure 3C) is indicative of a one-electron transfer reduction process involving the amine proton (NH). The reductive wave produced by the complex can be attributed to the reduction of Zn^{2+} to Zn^{+}, which is an irreversible one-electron transfer process. The dependence of the peak potential on scan rates indicates that only one electron is transferred, while the linearity of the plots of reduction peak

current, I_{pc} against scan rate, v for both the ligand and complex suggests that the electrode process was controlled by adsorption [44]. These results generally revealed that both the ligand and the complex are electrochemically active and this indicates they are biologically viable.

In vitro antibacterial activity

The results of antibacterial screening of the ligand, complex and the reference drug (streptomycin) obtained at concentrations of 10–30 µg.mL^{-1} using the agar diffusion method are presented in Figure 4. It is evident from this figure that the complex is more active against the tested organisms than the ligand and the reference drug. The complex appears to be more sensitive to the Gram-positive strains than the Gram-negative isolate, probably due to the variations in the complexities of the cell walls of the organisms. The zones of inhibition obtained shows that the antibacterial effect of the complex follows the order *S. aureus* > *S. pyogenes* > *K. pneumoniae* > *E. coli*, which indicates that the organisms were selectively affected, with *S. aureus* being the most susceptible, *E. coli* being the least while *S. pyogenes* and *K. pneumoniae* are both moderately affected. A similar trend is observed for the ligand with reduced zone of inhibition compared to the complex. This suggests that the complexation of the ligand with Zn(II) ion leads to enhanced bioactivity. Finally, the variation in the activity of the complex as a function of microbial strain could be attributed to varying degrees of cell permeability or difference in ribosome [45]. The results of the antimicrobial study correlate well with the results of cyclic voltammetric studies.

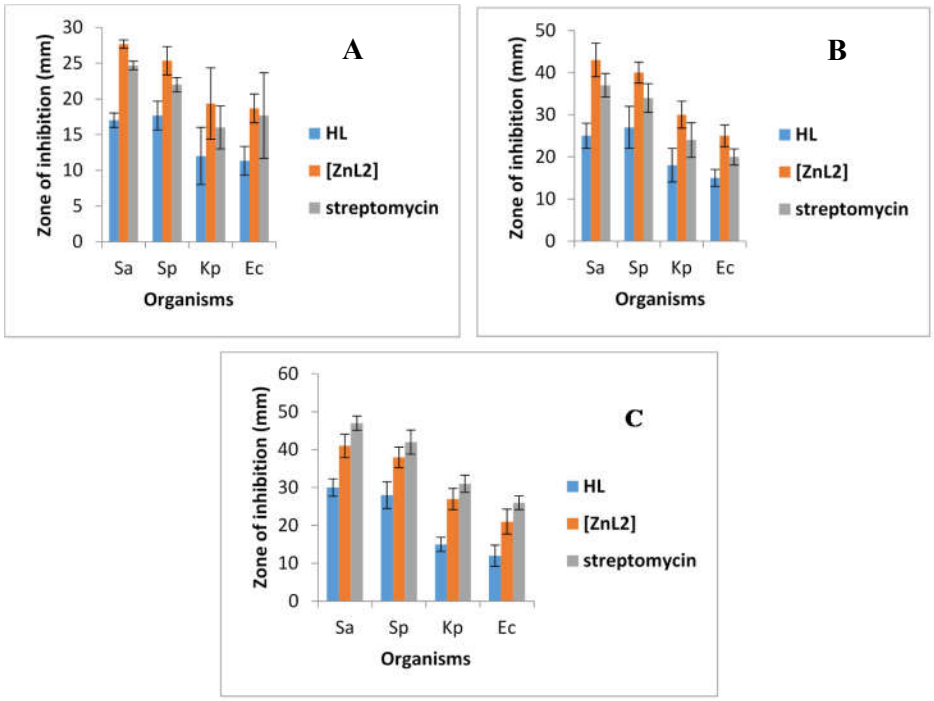

Figure 4. Comparison of *in vitro* antimicrobial activities of the ligands, the complex and the control drug on the studied bacteria at a concentration of 10 µg.mL^{-1} (A), 20 µg.mL^{-1} (B), and 30 µg.mL^{-1} (C); Sa: *S. aureus*, Sp: *S .pyogenes*, Ec: *E. coli*, and Kp: *K. pneumoniae*.

Minimum inhibitory concentration (MIC)

To further evaluate the antimicrobial potentials of the synthesized compounds, the minimum inhibitory concentrations (MIC) of the compounds were determined and compared with that of streptomycin. The data obtained revealed that the ligand exhibit moderate activity on the tested organisms. The ligand gave MICs of 64 $\mu g.mL^{-1}$ for *S. aureus* (Sa) and *S. pyogenes* (Sp), respectively, and 128 and 256 $\mu g.mL^{-1}$ for *K. pneumoniae* (Kp) and *E. coli* (Ec), respectively. The MIC values for the reference drug are 8 and 16 $\mu g.mL^{-1}$ for Sa and Sp, respectively, and 32 and 128 $\mu g.mL^{-1}$ for Kp and Ec. demonstrating that the ligand has the most effect on Sa and Sp, Kp has a moderate effect, and Ec has the least effect. The complex, on the other hand, gave MIC values of 32, 64, and 128 $\mu g.mL^{-1}$ for Sa and Sp, Kp, and Ec, respectively. This result indicates that complexation increases the antibacterial activity of the compound.

DFT-optimized geometries

The optimized geometries of ZnL_2 obtained with B3LYP, ωB97XD and M06-2X functionals are shown in Figure 5. From this figure, the values of a set of equivalent bond angles are listed in Table 1 to compare the relative performances of the functionals in predicting the geometry of the complex as proposed experimentally. These include N_2–Zn–O_4 and N_3–Zn–O_5, N_2–Zn–O_5 and N_3–Zn–O_4, and O_4–Zn–O_5 and N_2–Zn–N_3. Comparison of these pairs of bond angles shows that the B3LYP is the best performing functional as it yielded the most perfect geometry with the tetrahedral characteristics of a typical zinc (II) complex. The prediction strengths of the functionals follow the order B3LYP > ωB97XD > M06-2X.

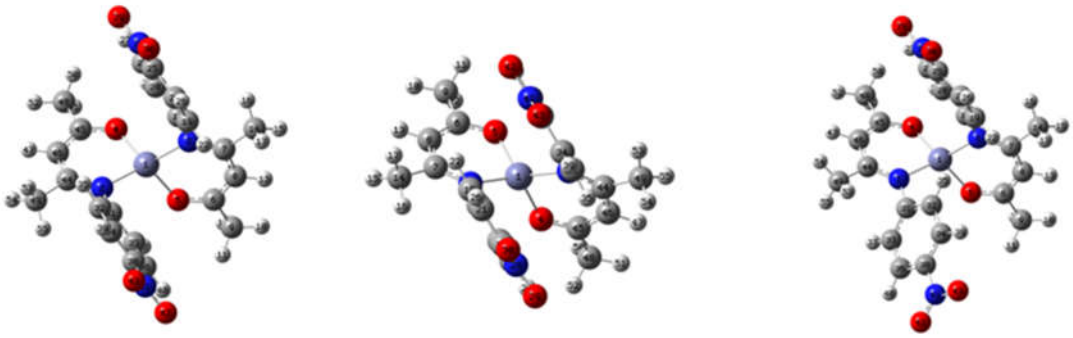

Figure 5. The optimized geometries of ZnL_2. Hydrogen, zinc, carbon, nitrogen and oxygen are coloured white, purple, grey, blue and red, respectively.

Table 1. Selected bond angles in the complex and the deviations of predicted IR frequencies.

	Bond angle(°)			
	B3LYP/6-31+G(d,p)/ LANL2DZ	ωB97XD/6-31+G(d,p)/ LANL2DZ		M06-2X/6-31+G(d,p)/ LANL2DZ
∠N_2–Zn–O_4	93.68	92.92		93.14
∠N_3–Zn–O_5	93.71	92.93		93.15
∠N_2–Zn–O_5	113.96	122.88		117.12
∠N_3–Zn–O_4	113.84	122.94		115.52
∠O_4–Zn–O_5	121.28	117.00		122.88
∠N_2–Zn–N_3	122.78	110.68		117.18

Deviations of predicted frequencies from experimental values (cm^{-1})						
Model	N-H	C=O	C-N	Zn-O	Zn-N	R^2
HL						
B3LYP/6-31+G(d,p)	138	12	24	–	–	1.000
ωB97XD/6-31+G(d,p)	264	22	51	–	–	1.000
M06-2X/6-31+G(d,p)	279	94	48	–	–	0.999
ZnL_2						
B3LYP/6-31+G(d,p)/ LANL2DZ	–	65	13	18	2	1.000
ωB97XD/6-31+G(d,p)/ LANL2DZ	–	52	14	29	10	0.999
M06-2X/6-31+G(d,p)/ LANL2DZ	–	54	18	32	24	0.999

DFT-predicted IR spectra

IR spectra and absorption frequencies were obtained from DFT calculations for both the ligand and the complex. The absolute deviations from the experimental values and the correlation coefficients (R^2) produced by each functional are given in Table 1 which clearly shows that the B3LYP model produced the least deviations and the best R^2 value (1.000). The performance strengths of the functionals rate as M06-2X < ωB97XD < B3LYP.

Reactivity properties of the studied compounds

Based on the outcome of geometry optimization and IR spectra prediction, the best performing functional (i.e. B3LYP) was selected for the reactivity and thermodynamic studies. The HOMO and LUMO charge density graphics are shown in Figure 6 for both the ligand and the complex. HOMO (i.e. highest occupied molecular orbital) is the orbital through which a molecule gives electron to an acceptor while LUMO is the one used for accepting an incoming electron. The higher the HOMO energy (E_{HOMO}), the greater the ease of giving an electron, and the lower the LUMO energy, the higher the likelihood of accepting an incoming electron. Thus, the E_{HOMO} and E_{LUMO} data (Figure 6) suggest that the complex will be a better electron donor and a better electron acceptor than the free ligand. This is in accord with the observed trend of redox behavior and bioactivity.

The energy of the LUMO relative to the HOMO gives the overall reactivity/stability of the molecule. The higher the HOMO-LUMO energy gap (ΔE_{HL}), the lower the reactivity and the higher the stability, and *vice versa*. The ΔE_{HL} values in Figure 6 further confirm the higher activity of the complex compared to the ligand. However, both of them are predicted to have comparable degrees of polarity hence, solubility as informed by their dipole moment (μ) values (6.96 and 6.95 Debye, for the ligand and the complex, respectively). The slight dipole moment difference suggests that the ligand may be slightly more soluble than the complex as confirmed by the experimental solubility trend discussed previously.

The HOMO and LUMO electron density isosurfaces reveal the parts of a molecule which might be involved in donation and acceptance of electrons, respectively. The HOMO isosurface of the ligand (Fig. 6) therefore indicates that the donating molecular orbital is distributed over the entire ligand structure with the exception of the methyl substituents. However, the carbonyl oxygen (O_{21}) and the amine nitrogen (N_{14}) atoms appear to be more susceptible to an electrophilic attack (i.e. donation to a metal ion) as informed by their natural charges of -0.643 and -0.598, respectively. On the other hand, the LUMO isosurface shows that the accepting orbital is mainly concentrated around the nitro phenyl portion of the molecule (Figure 6).

In the case of the complex, the HOMO isosurface is centered on the delocalized pi network between the carbonyl and the pseudo imine group of the attached ligand while the LUMO isosurface is spread over the nitro phenyl portions of the complex.

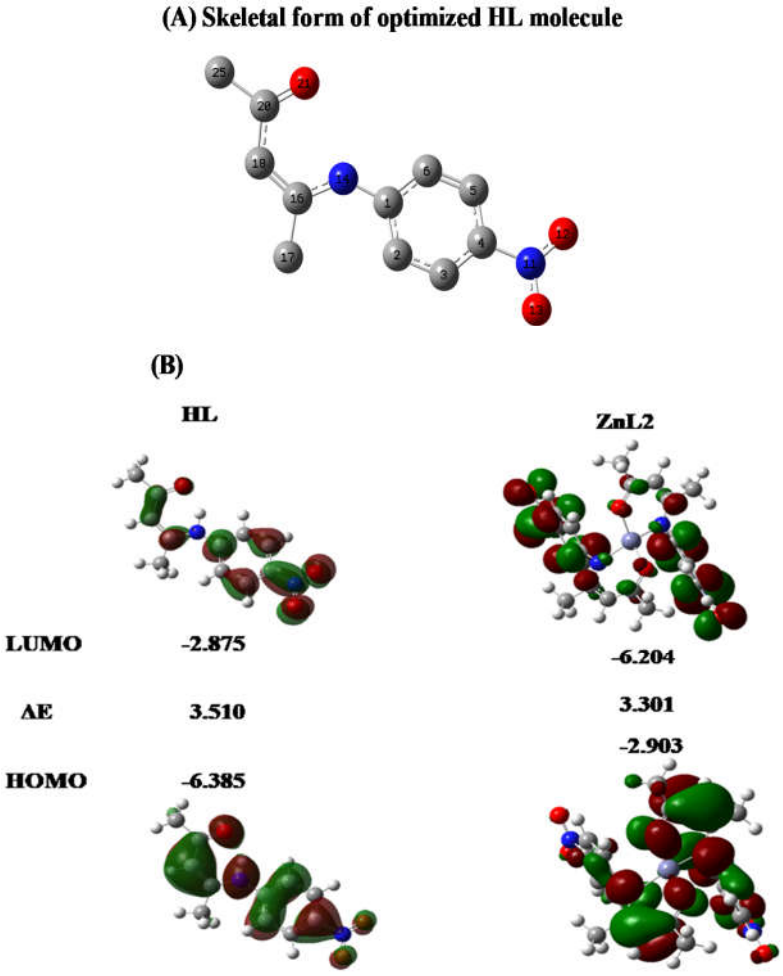

Figure 6. (A) Skeletal form of the optimized ligand and (B) HOMO and LUMO electron density isosurfaces of the ligand and the complex, as obtained from B3LYP calculation. Carbon, Oxygen and Nitrogen are coloured grey, red and blue, respectively.

Predicted thermodynamic properties of the complex at 298.15 K

Analysis of the thermodynamic parameters were obtained with DFT calculated ions shows that the formation of ZnL_2 is exothermic since it involves formation of new bonds between Zn(II) ion and two molecules of HL as indicated by the negative change in enthalpy of formation (ΔH = -1083.3 kJmol^{-1}). The negative change in entropy (ΔS = -348.72 kJmol^{-1}) implies that the complex formation is an associative process that resulted in a decrease in disorderliness. The negative

change in Gibb's free energy (ΔG = -979.33 kJmol^{-1}) suggests that the formation of ZnL_2 from Zn(II) ion and HL is highly spontaneous as it results in an increase in stability.

Molecular docking

The combination of *in silico* and *in vitro/in vivo* experimental processes has been described as an interesting strategy in the design and development of drug candidates [46]. In this study, the newly synthesized compounds were docked against key representative proteins in all the studied bacteria to predict their therapeutic potentials. Their free binding energies and conformations were determined and compared with that of the known antibacterial drug, streptomycin. The result presented in Table 2 shows that ZnL_2 might be a promising therapeutic candidate as revealed by its highest negative binding energy (ranging from -6.3 to -7.5 kcal.mol^{-1}) for the different proteins. The ligand, HL showed docking scores ranging from −5.4 to −7.1 kcal.mol^{-1} which was better than the interaction of streptomycin particularly in 6CN7.

Table 2. The binding affinities of the compounds with the studied proteins.

	HL		ZnL_2		Streptomycin	
PDB ID	BE (kcal/mol)	H-bond forming residue	BE (kcal/mol)	H-bond forming residue	BE (kcal/mol)	H-bond forming residue
1ESF	-5.4	Thr145, Asn146, Thr88	-6.3	Asn195	-5.6	Asn195, Gly200, Asp197
6OG4	-5.3	Lys223, Ala105, Ser112	-7.0	Val78	-5.9	Asn207, Lys208, Glu172, Glu103
6CN7	-7.1	Gln356, Arg145	-7.5	Gln424	-6.6	His422, Trp550, Asn425, Ser257, Arg259
1R4P	-6.7	Trp202, Gly203, Thr114	-7.3	Lys233	-6.6	Glu259, Asp94, Tyr77, Leu200, Asp111, Try114

The result for the binding interaction displayed in Figure 7 (for *S. aureus*) shows that the oxygen atoms of the nitro group of the HL share at least one hydrogen bond with the residues of the proteins. Similarly, Figure 7 shows that the oxygen atoms of both nitro and carbonyl groups of the ZnL_2 participated in the sharing of at least two hydrogen bonds with the amino acids of the studied protein. There was no comparable interaction observed between the standard drug molecule and the synthesized compounds except for ASN195 residue of 1ESF which participated in the complex formed with both ZnL_2 and streptomycin. Overall, the binding modes and interactions of the synthesized compounds across the proteins are different and stronger than the standard drug molecule. The involvement of different residues in the interactions could also suggest that the synthesized compounds might have a different mechanism of action from the known drug, streptomycin.

Drug-likeness and pharmacokinetic properties of the compounds

The calculated physicochemical properties and drug-likeness parameters of the synthesized compounds are enlisted in Table 3. Lipinski's requirements states that an orally active molecule should not violate any two of the physicochemical parameter range of MW ≤ 500, cLogP ≤ 5, HBDs ≤ 5, and HBAs ≤ 10. Veber also described TPSA and nRTBs values not more than 140 Å^2 and 10 respectively as efficient and selective criteria for oral bioavailability.

Furthermore, LogS has been described as one of the key parameters that facilitates the developmental activities of orally administered drugs [47, 48]. In this study, both HL and ZnL_2 complied with the RO_5 and Veber's rule. The LogS values also showed that both compounds might be soluble in water, in accord with the prediction of DFT. The results, therefore, imply that they have the prospect for good absorption and permeability across the membrane. Furthermore, the synthetic accessibility scores, 2.40 and 5.38 for HL and ZnL_2, respectively revealed that their molecular fragment might be easily obtainable.

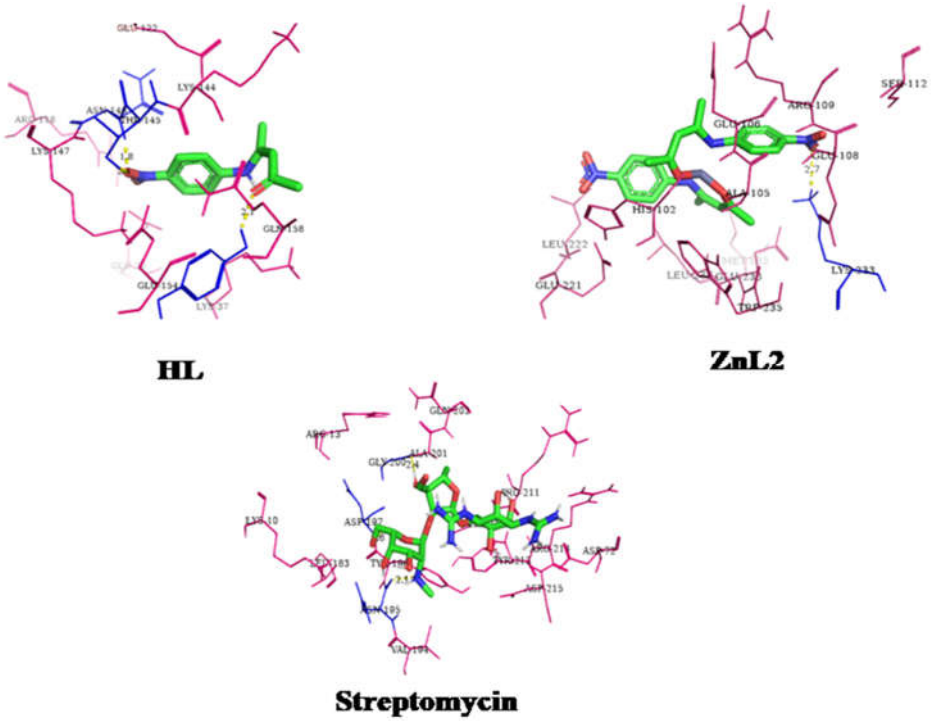

Figure 7. The interaction diagrams of HL, ZnL_2 and control (streptomycin) with the proteins from *S. aureus* (Sa). The polar (blue lines) and non-polar (pink lines) present residues of 1ESF, 6OG4, 6CN7 and 1R4P, respectively that were involved in the interaction. The yellow lines within the complexes represent hydrogen bonds and their respective distance.

The pharmacokinetic properties of the compounds are also described in Table 3. The results suggest that HL might be well absorbed while both compounds were predicted as non-P-substrates and they both showed the potential to penetrate the BBB. The compound, ZnL_2 showed inhibition of most of the CYP450 isozymes including CYP1A2, 2C19 and CYP3A4 while only CYP1A2, and CYP2C19 isozymes were inhibited by HL. Toxicity profiling showed that HL and ZnL_2 possess the risk of reproductive effects. This result implies the need for a more *in-vitro* assessment of the safety of these compounds.

Table 3. Selected molecular, physicochemical and pharmacokinetic properties of the ligand and its Zn(II) complex.

Molecular and physicochemical properties

Compounds	MW (≤500)	cLogP (≤ 5)	HBAs (≤ 10)	HBDs (≤ 5)	TPSA (≤ 140 Å²)	nRTBs (≤ 10)	LogS	SA	RO_5 rule	Veber rule
HL	220.22	1.6093	3	1	74.92 Å²	4	-2.78	2.40	Yes	Yes
ZnL_2	503.81	2.5486	6	0	132.26 Å²	4	-5.67	5.38	Yes	Yes

Pharmacokinetic properties

Compounds	GI absorption	P-gp substrate	BBB permeate	CYP1A2 inhibitor	CYP2C19 inhibitor	CYP2C9 inhibitor	CYP2D6 inhibitor	CYP3A4 inhibitor	Mutagenic	Tumorigenic	Reproductive effects	Irritants
HL	High	No	Yes	Yes	Yes	No	No	No	No	High	No	No
ZnL_2	Low	No	Yes	No	Yes	Yes	No	Yes	No	High	No	No

MW: Molecular weight, cLogP: calculated log of octanol/water partition coefficient, HBAs: Hydrogen bond acceptors, HBDs: Hydrogen bond donors, TPSA: Total polar surface area nRTBs: Number of rotatable bonds, Log S: log of solubility. RO_5; Rule of five; GI: Gastrointestinal, P-gp: *p*-glyco-proteins, BBB: Blood-brain barrier, CYP: Cytochrome P450

CONCLUSION

β-Ketoamine Schiff base ligand, ((*Z*)-4-((4-nirophenyl)amino)pent-3-en-2-one), was synthesized from acetylacetone and 4-nitroaniline, and complexed with Zn(II) ion. The compositions and structures of the ligand and its Zn(II) complex were confirmed using analytical and physicochemical analyses. From these analyses, it was discovered that the ligand acted as a bidentate and coordinated to the Zn(II) ion via the oxygen and nitrogen atoms of the carbonyl and amine functional groups, respectively, resulting in a tetrahedral geometry. The antimicrobial activity results showed that the complex outperformed the ligand, and that the activity was concentration-dependent. The results of DFT study correlated well with the experimental data and also revealed electronic properties that supported the biological activities of the compounds. Furthermore, molecular docking study revealed a range of potential interactions with principal binding protein-sites in the studied bacteria and correlated well with the experimental results (MIC and zone of inhibition). The compounds were predicted by in silico ADMET studies to possess good drug-like properties. This provides a strong basis for a medicinal chemistry approach to fine-tune the characteristics and activity of the compounds.

ACKNOWLEDGEMENT

The authors would like to thank Dr. L.O. Olasunkanmi of Obafemi Awolowo University, Ile-Ife, Nigeria, for providing access to necessary computational facilities.

REFERENCES

1. More, M.; Joshi, P.; Mishra, Y.; Khanna, P. Metal complexes driven from Schiff bases and semicarbazones for biomedical and allied applications: A review. *Mater. Today Chem.* **2019**, 14, 100195.
2. Hashem, H.E.; Mohamed, E.A.; Farag, A.A.; Negm, N.A.; Azmy, EA. New heterocyclic Schiff base-metal complex: Synthesis, characterization, density functional theory study, and antimicrobial evaluation. *Appl. Organomet. Chem.* **2021**, 35, e6322.

3. Yaşar, Ü.; Gönül, İ.; Türkeş, C.; Demir, Y.; Beydemir, Ş. Transition metal complexes of bidentate Schiff base ligands: In vitro and in silico evaluation as non-classical carbonic anhydrase and potential acetylcholinesterase inhibitors. *Chem. Select*. **2021**, 6, 7278-7284.
4. Ventola, C.L. The antibiotic resistance crisis: Part 1: Causes and threats. *Pharm. Ther*. **2015**, 40, 277-283.
5. Berhe, D.F.; Beyene, G.T., Seyoum, B.; Gebre, M.; Haile, K., Tsegaye, M.; Boltena, M.T.; Tesema, E.; Kibret, T.C.; Biru, M.; Siraj, D.S.; Prevalence of antimicrobial resistance and its clinical implications in Ethiopia: A systematic review. *Antimicrob. Resist. Infect. Control* **2021**, 10, 1-14.
6. Cave, R.; Cole, J.; Mkrtchyan, HV. Surveillance and prevalence of antimicrobial resistant bacteria from public settings within urban built environments: Challenges and opportunities for hygiene and infection control. *Environ. Intel*. **2021**, 157, 106836.
7. Tadesse, B.T.; Ashley, E.A.; Ongarello, S.; Havumaki, J.; Wijegoonewardena, M.; González, I.J.; Dittrich, S. Antimicrobial resistance in Africa: a systematic review. *BMC Infect. Dis*. **2017**, 17, 1-17.
8. Ahmad, N.; Alam, M.; Wahab, R.; Ahmed, M.; Ahmad, A. Synthesis, spectral and thermo-kinetics explorations of Schiff-base derived metal complexes. *Open Chem*. **2020**, 18, 1304-1315.
9. Pettinari, R.; Pettinari, C.; Marchetti, F.; Clavel, C.M.; Scopelliti, R.; Dyson, P.J. Cytotoxicity of ruthenium–arene complexes containing β-ketoamine ligands. *Organomet*. **2013**, 32, 309-316.
10. Kianfar, A.H.; Fath, R.H. Theoretical study of the structures of Schiff base compounds and thermodynamic study of the tautomerism reactions by ab initio calculations. *Egypt. J. Pet*. **2017**, 26, 865-874.
11. Belkasem, H.; Desouky, O. Preparation of Schiff bases complexes derived from acetyl acetone with benzidine, *p*-phenylenediamine, *p*-toluidine and aniline with some transition metal ions (II) and (III). *J. Agric. Chem. Biotecnol*. **2010**, 1, 621-628.
12. Hosny, N.M.; Hussien, M.A.; Radwan, F.M.; Nawar, N. Synthesis, spectral, thermal and optical properties of Schiff base complexes derived from 2 (E)-2-((z)-4-hydroxypent-3-en-2-ylideneamino)-5-guanidinopentanoic acid and acetylacetone. *J. Mol. Struct*. **2017**, 1143, 176-183.
13. Patil, S.A.; Medina, P.A.; Gonzalez-Flores, D.; Vohs, J.K.; Dever, S.; Pineda, L.W.; Montero, M.L.; Fahlman, B.D. Formic Acid: A low-cost, mild, ecofriendly, and highly efficient catalyst for the rapid synthesis of β-enaminones. *Synth. Commun*. **2013**, 43, 2349-2364.
14. Saadat, A.; Banaei, A.; Mcardle, P.; Jafari, R. Spectral, structural, and antibacterial study of copper(II) complex with N_2O_2 donor Schiff base ligand and its usage in preparation of CuO nanoparticles. *J. Chem*. **2022**, 2022, 1-13. https://doi.org/10.1155/2022/8913874.
15. Singh, R.K; Prasad, D.; Bhardwaj, T. Design, synthesis and in vitro cytotoxicity study of benzodiazepine-mustard conjugates as potential brain anticancer agents. *J. Saudi Chem. Soc*. **2017**, 1, S86-S93.
16. Becke, A.D. Density-functional thermochemistry. I. The effect of the exchange only gradient correction. *J. Chem. Phys*. **1992**, 96, 2155-2160.
17. Lee, C.; Yang, W.; Parr, R.G. Development of the Colle-Salvetti correlation energy formula into a functional of the electron density. *Phys. Rev B*. **1988**, 37, 785-789.
18. Chai, J.D.; Head-Gordon, M. Long-range corrected hybrid density functionals with damped atom–atom dispersion corrections. *Phys. Chem. Chem. Phys*. **2008**, 10, 6615-6620.
19. Zhao, Y.; Truhlar, D.G. The M06 suite of density functionals for main group thermochemistry, thermochemical kinetics, noncovalent interactions, excited states, and transition elements: Two new functionals and systematic testing of four M06-class functionals and 12 other functionals. *Theor. Chem. Acc*. **2008**, 120, 215-241.

20. Olasunkanmi, L.O.; Idris, A.O.; Adewole, A.H.; Wahab, O.O.; Ebenso, E.E. Adsorption and corrosion inhibition potentials of salicylaldehyde-based Schiff bases of semicarbazide and *p*-toluidine on mild steel in acidic medium: Experimental and computational studies. *Surf. Interface* **2020**, 21, 100782.
21. Cances, E.; Mennucci, B.; Tomasi, J. A new integral equation formalism for the polarizable continuum model: Theoretical background and applications to isotropic and anisotropic dielectrics. *J. Chem. Phys*. **1997**, 107, 3032-3041.
22. Frisch, M.; Trucks, G.; Schlegel, H.; Scuseria, G.; Robb, M.; Cheeseman, J. *Gaussian 09, Revision B. 01. Gaussian 09, Revision B. 01*, Gaussian Inc: Wallingford CT; **2009**.
23. Wahab, O.O.; Olasunkanmi, L.O.; Govender, K.K.; Govender, P.P. Synergistic effect of opposite polar substituents on selected properties of disperse yellow 119 dye. *Chem. Phys. Lett*. **2018**, 704, 55-61.
24. Wahab, O.O.; Olasunkanmi, L.O.; Govender, K.K.; Govender, PP. Tuning the aqueous solubility, chemical reactivity and absorption wavelength of azo dye through systematic adjustment of molecular charge density: a DFT study. *Mol. Phys*. **2020**, 118, e1626508.
25. Butt, S.S.; Badshah, Y.; Shabbir, M.; Rafiq, M. Molecular docking using chimera and autodock vina software for nonbioinformaticians. *JMIR Bioinform. Biotech*. **2020**, 1, e14232.
26. Dallakyan, S.; Olson, A.J. *Small-molecule library screening by docking with PyRx* in *Chem. Bio.*: Springer: Berlin; **2015**, pp. 243-250.
27. Shaker, B.; Yu, M-S.; Lee, J.; Lee, Y.; Jung, C.; Na, D. User guide for the discovery of potential drugs via protein structure prediction and ligand docking simulation. *J. Microbiol*. **2020**, 58, 235-244.
28. Seeliger, D.; de Groot, B.L. Ligand docking and binding site analysis with PyMOL and Autodock/Vina. *J. Comput. Aided Mol. Des*. **2010**, 24, 417-422.
29. Daina, A.; Michielin, O.; Zoete, V. SwissADME: A free web tool to evaluate pharmacokinetics, drug-likeness and medicinal chemistry friendliness of small molecules. *Sci. Rep*. **2017**, 7, 1-13.
30. Oselusi, S.O.; Christoffels, A., Egieyeh, S.A. Cheminformatic characterization of natural antimicrobial products for the development of new lead compounds. *Molecule* **2021**, 26, 3970.
31. Sander, T.; Freyss, J.; von Korff, M.; Rufener, C. DataWarrior: An open-source program for chemistry aware data visualization and analysis. *J. Chem. Inf. Model*. **2015**, 55, 460-473.
32. Mills, N. ChemDraw Ultra 10.0 CambridgeSoft, 100 Cambridge Park Drive, Cambridge, MA 02140. www. cambridgesoft. com. Commercial Price: 1910 for download, 2150 for CD-ROM; Academic Price: 710 for download, 800 for CD-ROM. *ACS Pub*. **2006**, 13649-13650
33. Lipinski, C.A. *Physicochemical properties and the discovery of orally active drugs: Technical and people issues* in *Molecular Informatics: Confronting Complexity, Proceedings of the Beilstein-Institut Workshop*, Frankfurt, Germany; **2003**.
34. Oselusi, S.O.; Egieyeh, S.A.; Christoffels, A. Cheminformatic profiling and hit prioritization of natural products with activities against methicillin-resistant *Staphylococcus aureus* (MRSA). *Molecule* **2021**, 26, 3674.
35. Ali, I.; Wani, W.A.; Saleem, K. Empirical formulae to molecular structures of metal complexes by molar conductance. *Synth. React. Inorg. Met-Org. Nano-Met. Chem*. **2013**, 43, 1162-1170.
36. Gordon, A.T.; Abosede, O.O.; Ntsimango, S.; van Vuuren, S.; Hosten, E.C.; Ogunlaja, A.S. Synthesis, characterization, molecular docking and antimicrobial activity of copper(II) complexes of metronidazole and 1,10 phenanthroline. *Inorg Chim. Acta* **2020**, 510, 119744.
37. Hernández-Morales, A.; Rivera, J.M.; López-Monteon, A.; Lagunes-Castro, S.; Castillo-Blum, S.; Cureno-Hernandez, K.*;* Flores-Parra, A.; Villasenor-Granados, O.; Colorado-Peralta, R. Complexes containing benzimidazolyl-phenol ligands and Ln(III) ions: synthesis, spectroscopic studies and preliminary cytotoxicity evaluation. *J. Inorg. Biochem.* **2019**, 201, 110842.

38. Zhang, X.Z.; Li, L.X.; Li, H.H.; You, Z.; Zhu, H.L. Synthesis, characterization and crystal structures of oxovanadium(V) complexes derived from similar aroylhydrazone ligands. *Bull. Chem. Soc. Ethiop.* **2015**, 29, 423-430.
39. Srivastva, A.N.; Singh, N.P.; Shriwastaw, C.K. In vitro antibacterial and antifungal activities of binuclear transition metal complexes of ONNO Schiff base and 5-methyl-2,6-pyrimidine-dione and their spectroscopic validation. *Arab. J. Chem.* **2016**, 9, 48-61.
40. El-Tabl, A.S.; Mohamed, A.M.; Wahba, M.A.; Abou, E.A.H. Synthesis, characterization, and anticancer activity of new metal complexes derived from 2-hydroxy-3-(hydroxyimino)-4-oxopentan-2-ylidene)benzohydrazide. *Bioinorg. Chem. Appl.* **2015**, 2015, 1-14. http://dx.doi.org/10.1155/2015/12602.
41. Raman, N.; Ravichandran, S.; Thangaraja, C. Copper(II), cobalt(II), nickel(II) and zinc(II) complexes of Schiff base derived from benzil-2,4-dinitrophenylhydrazone with aniline. *J. Chem. Sci.* **2004**, 116, 215-219.
42. Waziri, I.; Ndahi, N.P.; Paul, B. Synthesis, physicochemical and antimicrobial studies of Co(II), Zn(II) and Fe(III) mixed antibiotics metal complexes. *J. Chem. Pharm. Res.* **2013**, 5, 84-89.
43. Bal, M.; Ceyhan, G.; Avar, B.; Köse, M.; Kayraldiz, A.; Kurtoğlu, M. Synthesis and X-ray powder diffraction, electrochemical, and genotoxic properties of a new azo-Schiff base and its metal complexes. *Turk. J. Chem.* **2014**, 38, 222-241.
44. El-Maali, N.A.; Osman, A.; Aly, A.; Al-Hazmi, G. Voltammetric analysis of Cu(II), Cd(II) and Zn(II) complexes and their cyclic voltammetry with several cephalosporin antibiotics. *Bioelectrochem.* **2005**, 65, 95-104.
45. Sengupta, S.K.; Pandey, O.P.; Srivastava, B.K.; Sharma, V.K. Synthesis, structural and biochemical aspects of titanocene and zirconocene chelates of acetylferrocenyl thiosemicarbazones. *Transit. Met. Chem.* **1998**, 23, 349-353.
46. Brogi, S.; Ramalho, T.C.; Kuca, K.; Medina-Franco, J.L.; Valko, M. In silico methods for drug design and discovery. *Front. Chem.* **2020**, 8, 612.
47. Keivanloo, A.; Abbaspour, S.; Sepehri, S.; Bakherad, M. Synthesis, antibacterial activity and molecular docking study of a Series of 1, 3-oxazole-quinoxaline Amine Hybrids. *Polycy. Aromat. Cpds.* **2020**, 42, 1-14.
48. Craciun, D.; Modra, D.; Isvoran, A. *ADME-Tox profiles of some food additives and pesticides* in *AIP Conference Proceedings*: AIP Publishing LLC; **2015**. p. 040007.